Taylor & Francis
Taylor & Francis Group

Journal of Enzyme Inhibition and Medicinal Chemistry

ISSN: 1475-6366 (Print) 1475-6374 (Online) Journal homepage: http://www.tandfonline.com/loi/ienz20

Targeting clinically-relevant metallo-β-lactamases: from high-throughput docking to broad-spectrum inhibitors

Margherita Brindisi, Simone Brogi, Simone Giovani, Sandra Gemma, Stefania Lamponi, Filomena De Luca, Ettore Novellino, Giuseppe Campiani, Jean-Denis Docquier & Stefania Butini

To cite this article: Margherita Brindisi, Simone Brogi, Simone Giovani, Sandra Gemma, Stefania Lamponi, Filomena De Luca, Ettore Novellino, Giuseppe Campiani, Jean-Denis Docquier & Stefania Butini (2016): Targeting clinically-relevant metallo-β-lactamases: from high-throughput docking to broad-spectrum inhibitors, Journal of Enzyme Inhibition and Medicinal Chemistry, DOI: 10.3109/14756366.2016.1172575

To link to this article: http://dx.doi.org/10.3109/14756366.2016.1172575

Published online: 28 Apr 2016.

Submit your article to this journal

View related articles

View Crossmark data

Full Terms & Conditions of access and use can be found at
http://www.tandfonline.com/action/journalInformation?journalCode=ienz20

Download by: [Universita degli Studi di Siena] **Date:** 28 April 2016, At: 03:47

Journal of Enzyme Inhibition and Medicinal Chemistry

www.tandfonline.com/ienz
ISSN: 1475-6366 (print), 1475-6374 (electronic)

J Enzyme Inhib Med Chem, Early Online: 1–12
© 2016 Informa UK Limited, trading as Taylor & Francis Group. DOI: 10.3109/14756366.2016.1172575

Taylor & Francis
Taylor & Francis Group

RESEARCH ARTICLE

Targeting clinically-relevant metallo-β-lactamases: from high-throughput docking to broad-spectrum inhibitors

Margherita Brindisi[1,2], Simone Brogi[1,2], Simone Giovani[1,2], Sandra Gemma[1,2], Stefania Lamponi[1,2], Filomena De Luca[3], Ettore Novellino[4], Giuseppe Campiani[1,2], Jean-Denis Docquier[3], and Stefania Butini[1,2]

[1]European Research Centre for Drug Discovery and Development (NatSynDrugs), University of Siena, Siena, Italy, [2]Department of Biotechnology, Chemistry and Pharmacy, University of Siena, Siena, Italy, [3]Department of Medical Biotechnology, University of Siena, Siena, Italy, and [4]Department of Pharmacy, University of Napoli Federico II, Napoli, Italy

Downloaded by [Universita degli Studi di Siena] at 03:47 28 April 2016

Abstract

Metallo-β-lactamases (MBLs) represent one of the most important and widespread mechanisms of resistance to β-lactam antibiotics (including the life-saving carbapenems), against which no clinically useful inhibitors are currently available. We report herein a structure-based high-throughput docking (HTD) campaign on three clinically-relevant acquired MBLs (IMP-1, NDM-1 and VIM-2). The initial hit NF1810 (**1**) was optimized providing the broad-spectrum inhibitor **3i**, which is able to potentiate the *in vitro* activity of cefoxitin on a VIM-2-producing *E. coli* strain.

Keywords

Antibiotic resistance, docking, metallo-β-lactamase

History

Received 8 February 2016
Revised 22 March 2016
Accepted 23 March 2016
Published online 26 April 2016

Introduction

Gram-negative bacteria show a steady rising inclination to antibiotic resistance, and have successfully evolved towards extensively-drug resistance (XDR) or even pan-drug resistance (PDR) phenotypes, and thus can be responsible for infections that result extremely difficult or impossible to treat with currently-available antibiotics[1]. Carbapenems, the last generation of β-lactam antibiotics, represent the main choice for the treatment of serious infections caused by multidrug-resistant Gram-negative pathogens[2]. However, their widespread medical use over more than two decades has contributed to the evolution of several bacterial resistance mechanisms to carbapenems and other β-lactams. Several clinically-relevant Gram-negative pathogens (carbapenem-resistant *Klebsiella pneumoniae*, *Acinetobacter baumannii*, *Pseudomonas aeruginosa*, and *Enterobacter* spp.) – included among the acronymically dubbed ''ESKAPE pathogens'' – have become highly-resistant to the vast majority of available antibacterial drugs and are able to dodge the biocidal action of antibiotics[3,4]. Therefore, facing the mounting threat of antimicrobial resistance today represents a great challenge for clinicians and medicinal chemists. One important mechanism of resistance to β-lactams[5] is the production of one or more β-lactamase(s), which efficiently inactivate these antibiotics[6,7]. The global spread of extended-spectrum β-lactamases (ESBLs) led to increased use of carbapenems, broad-spectrum antibiotics which are stable to ESBLs. This event in turn elicited the appearance of carbapenemase-producing clinical isolates, belonging to either the active serine enzymes (e.g. KPC-2, OXA-48) or the metallo-β-lactamases (MBLs) (e.g. IMP-1, VIM-2, NDM-1)[8–10]. Considering their structural heterogeneity, MBLs are divided into three distinct subclasses (B1, B2 and B3)[11]. Subclass B1 enzymes, which include most of the clinically-important enzymes, have a dinuclear zinc-containing active site. The first zinc site is coordinated by three His residues and the second by a Asp-Cys-His triad. MBLs are encoded by mobile genetic elements, responsible for their diffusion in various Gram-negative pathogens. In particular NDM-1-producing isolates have shown, since the first report in 2008, a rapid and worldwide spread, presenting a high risk of a worldwide pandemia among *Enterobacteriaceae* and causing a global concern[12]. Furthermore, the diffusion of MBL-producing isolates of *Pseudomonas aeruginosa*, a bacterial pathogen of primary relevance for both nosocomial and chronic infections of the respiratory tracts in cystic fibrosis patients, is notably increasing in some specific settings[13]. While inhibitors of serine β-lactamases are currently available in the clinical practice (clavulanic acid, sulbactam, tazobactam and avibactam), no clinically useful inhibitors of MBLs have been developed yet[10]. As a consequence, there is an urgent need to identify clinically useful MBL inhibitors, that could be amenable to clinical development to be given in combination with existing β-lactams. Preferably, these inhibitors should be effective against multiple MBL subgroups and variants[2,14]. In this paper, we report a structure-based high-throughput docking (HTD) on three clinically-relevant MBLs which led to the discovery of the hit compound **1** (Figure 1). The structure–activity relationship (SAR) studies performed on the hit

Address for correspondence: Sandra Gemma, European Research Centre for Drug Discovery and Development (NatSynDrugs), University of Siena, via Aldo Moro 2, Siena 53100, Italy. E-mail: gemma@unisi.it; Giuseppe Campiani, European Research Centre for Drug Discovery and Development (NatSynDrugs), University of Siena, via Aldo Moro 2, Siena 53100, Italy. E-mail: campiani@unisi.it

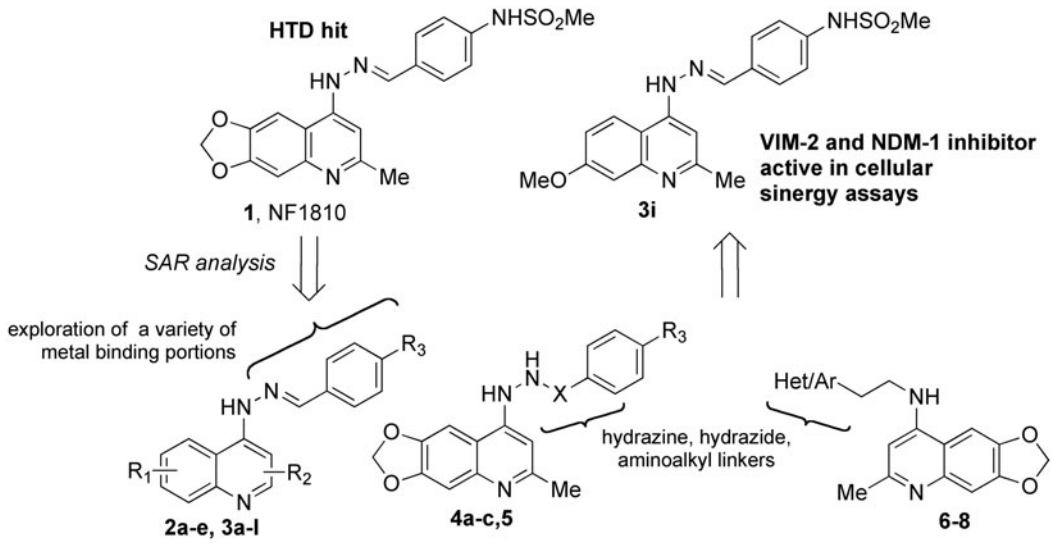

Figure 1. Structure of the HTD hit compound **1**, of the optimized derivative **3i** and general structure of inhibitors identified in this study.

Downloaded by [Universita degli Studi di Siena] at 03:47 28 April 2016

compound (**2a–e**, **3a–l**, **4a–c** and **5–8**, Figure 1) led to the selection of a broad-spectrum inhibitor (**3i**) which was microbiologically evaluated to confirm its ability in potentiating the efficacy of the antibiotic cefoxitin on a VIM-2-producing *E. coli* strain.

Materials and methods

Chemistry

Unless otherwise specified, materials were purchased from commercial suppliers and used without further purification. Reaction progress was monitored by TLC using silica gel 60 F254 (0.040–0.063 mm) by UV detection. Silica gel 60 (0.040–0.063 mm) was used for column chromatography. ^{1}H NMR spectra were recorded on a Varian 300 MHz spectrometer (Varian Inc., Palo Alto, CA) or a Bruker 400 MHz spectrometer (Bruker Corp., Billerica, MA) by using the residual signal of the deuterated solvent as internal standard. Splitting patterns are described as singlet (s), doublet (δ), triplet (t), quartet (q) and broad (br); the value of chemical shifts (δ) are given in ppm and coupling constants (J) in Hertz (Hz). ESI-MS spectra were performed by an Agilent 1100 Series LC/MSD spectrometer (Agilent Technologies, Santa Clara, CA). Melting points were determined in Pyrex capillary tubes using an Electrothermal 8103 apparatus and are uncorrected. Yields refer to purified products and are not optimized. Elemental analyses were performed in a Perkin Elmer 240C elemental analyser (Perkin Elmer, Waltham, MA) and the results were within ±0.4% of the theoretical values.

Hydrazones **1** and **2a–e** were prepared as previously described[15]. Hydrazines **9a–g** were prepared following described procedures[15–18]. Non-commercially available aldehydes **10a,b** were prepared following reported procedures[19,20]. Piperazines **15**,**16** were prepared following described procedures[21,22].

General procedure for the synthesis of hydrazones 3a–l

*4-((2-(6-Methyl-[1,3]dioxolo[4,5-g]quinolin-8-yl)hydrazono) methyl)benzenesulfonamide (**3a**)*

Hydrazine **9a** and aldehyde **10a** in an equimolar ratio were suspended in absolute ethanol and the mixture was refluxed for 16 h. Solvent was then evaporated *in vacuo*. The crude product was purified by chromatography on silica gel (gradient elution from 100% $CHCl_3$ to 20% MeOH in $CHCl_3$) to afford the title compound as a brown powder (60 mg, 23% yield); ^{1}H NMR: (DMSO-d_6, 300 MHz) δ 3.29 (s, 3H), 6.14 (s, 2H), 7.13 (s, 1H), 7.21 (s, 1H), 7.39 (s, 2H), 7.66 (s, 1H), 7.84 (d, $J = 7.8$ Hz, 2H), 7.91 (d, $J = 8.1$ Hz, 2H), 8.32 (s, 1H), 10.90 (s, 1H); ^{13}C NMR: (DMSO-d_6, 75 MHz) δ 25.4, 97.9, 101.3, 102.4, 105.7, 111.3, 126.8 (2C), 127.3 (2C), 138.9, 140.8, 144.5, 146.5, 146.9, 150.5, 157.2; ESI MS *m/z*: 385 $[M + H]^+$.

*N-(4-((2-([1,3]Dioxolo[4,5-g]quinolin-8-yl)hydrazono)methyl)-phenyl)methanesulfonamide (**3b**)*

Starting from hydrazine **9b** and aldehyde **10b**, compound **3b** was obtained following the procedure developed for **3a** (16 mg, 7% yield); ^{1}H NMR: (CD_3OD, 300 MHz) δ 3.00 (s, 3H), 6.22 (s, 2H), 7.19 (s, 1H), 7.33 (d, $J = 8.7$ Hz, 2H), 7.53 (d, $J = 6.6$ Hz, 1H), 7.70 (s, 1H), 7.78 (d, $J = 8.7$ Hz, 2H), 8.29 (s, 1H), 8.31 (s, 1H); ^{13}C NMR: (CD_3OD, 75 MHz) δ 29.4, 38.4, 78.2, 97.6, 100.2, 103.2, 111.9, 119.4, 128.3, 130.3, 140.4, 142.7, 146.1, 148.5, 150.4, 152.9; ESI MS *m/z*: 385 $[M + H]^+$.

*8-(2-(4-(Methylthio)benzylidene)hydrazinyl)-[1,3]dioxolo[4,5-g] quinoline (**3c**)*

Starting from hydrazine **9b** and aldehyde **10c,** compound **3c** was obtained following the procedure developed for **3a** (15 mg, 23% yield); ^{1}H NMR: (CD_3OD, 300 MHz) δ 2.51 (s, 3H), 6.12 (s, 2H), 7.15 (s, 1H), 7.29 (d, $J = 8.1$ Hz, 2H), 7.37 (d, $J = 5.4$ Hz, 1H), 7.55 (s, 1H), 7.67 (d, $J = 8.4$ Hz, 2H), 8.16 (s, 1H), 8.29 (d, $J = 5.4$ Hz, 1H); ESI MS *m/z*: 338 $[M + H]^+$.

*N-(4-((2-(1,2,3,4-Tetrahydroacridin-9-yl)hydrazono)methyl) phenyl)methanesulfonamide (**3d**)*

Compound **3e** was obtained starting from hydrazine **9c** and aldehyde **10b** following the same synthetic strategy described for **3a**. A 0 °C filtration of the reaction mixture provided the title compound as a yellow powder without any further purification (46 mg, 80% yield); ^{1}H NMR: (CD_3OD, 300 MHz) δ 1.91–1.95 (m, 4H), 2.89 (s, 2H), 3.01 (s, 5H), 7.31 (d, $J = 8.7$ Hz, 2H), 7.48 (t, $J = 1.8$ Hz, 1H), 7.66–7.77 (m, 3H), 7.89 (s, 1H), 8.28 (s, 1H), 9.11 (d, $J = 8.7$ Hz, 1H); ^{13}C NMR: (DMSO-d_6, 75 MHz) δ 21.1,

Downloaded by [Universita degli Studi di Siena] at 03:47 28 April 2016

22.2, 25.3, 29.3, 49.3, 111.8, 116.3, 119.8 (2C), 120.4, 126.1, 128.0, 129.2 (2C), 129.4, 132.9, 139.5, 141.3, 149.5, 149.9, 152.7; ESI MS *m/z*: 395 $[M+H]^+$.

*2-(4-(Dimethoxymethyl)benzylidene)-1-(6-methyl[1,3]dioxolo [4,5-g]quinolin-8-yl)hydrazine (**3e**)*

To a solution of **2e**[15] (50 mg, 0.15 mmol) in MeOH, a catalytic amount of HBF_4 was added. There was a immediate precipitation of a light yellow solid that was filtered and washed with MeOH to obtain pure acetal **3e**, without the necessity of further purifications (54 mg, 95% yield); ^{1}H NMR: (CD_3OD, 300 MHz) δ 2.69 (s, 3H), 3.28–3.35 (m, 8H), 5.42 (s, 1H), 6.2 (s, 2H), 7.16 (s, 1H), 7.54 (d, $J=8.2$ Hz, 2H), 7.75 (s, 1H), 7.85 (d, $J=7.8$ Hz, 2H), 8.43 (s, 1H); ESI MS *m/z*: 380 $[M+H]^+$.

*9-(2-(4-(Methylthio)benzylidene)hydrazinyl)-1,2,3,4-tetrahydroacridine (**3f**)*

Compound **3f** was obtained starting from hydrazine **9c** and aldehyde **10c** following the same synthetic strategy described for **3a.** Yield: 47%; ^{1}H NMR: (CD_3OD, 300 MHz) δ 1.89–2.05 (m, 4H), 2.51 (s, 3H), 2.85 (d, $J=9.1$ Hz, 2H), 3.14 (d, $J=9.1$ Hz, 2H), 7.36 (d, $J=8.4$ Hz, 2H), 7.64 (t, $J=7.2$ Hz, 1H), 7.72 (d, $J=8.4$ Hz, 2H), 7.79 (d, $J=7.8$ Hz, 1H), 7.87 (t, $J=7.5$ Hz, 1H), 8.48 (s, 1H), 9.44 (d, $J=8.7$ Hz, 1H); ^{13}C NMR: (CD_3OD, 75 MHz) δ 13.7, 20.7, 21.8 (2C), 24.0, 28.6, 111.1, 116.1, 119.0, 125.6, 125.8 (2C), 127.8 (2C), 128.1, 130.2, 132.9, 143.5, 150.0, 150.2, 152.1; ESI MS *m/z*: 348 $[M+H]^+$.

*N-(4-((2-(6-Methoxy-2-methylquinolin-4-yl)hydrazono)methyl)-phenyl)methanesulfonamide (**3g**)*

Compound **3g** was obtained starting from hydrazine **9d** and aldehyde **10b** following the same synthetic strategy described for **3a.** Yield: 25%; ^{1}H NMR: (CD_3OD, 300 MHz) δ 2.57 (s, 3H), 3.00 (s, 3H), 3.95 (s, 3H), 7.50–7.52 (m, 1H), 7.74–7.26 (m, 4H), 7.72 (t, $J=8.4$ Hz 3H), 8.23 (s, 1H). ^{13}C NMR: (CD_3OD, 75 MHz) δ 22.8, 38.3, 55.1, 99.9, 101.2, 116.5, 119.8, 121.6, 127.5, 127.8, 131.2, 140.0, 142.5, 143.0, 148.1, 155.9, 157.0; ESI MS *m/z*: 385 $[M+H]^+$.

*6-Methoxy-2-methyl-4-(2-(4-(methylthio)benzylidene)hydrazinyl)-quinoline (**3h**)*

Starting from hydrazine **9d** and aldehyde **10c**, title compound was obtained following the procedure developed for **3a** (12 mg, 26% yield); ^{1}H NMR: ($CDCl_3$, 300 MHz) δ 2.50 (s, 3H), 2.59 (s, 3H), 3.96 (s, 3H), 7.37–7.28 (m, 4H), 7.56–7.54 (m, 1H), 7.76–7.68 (m, 3H), 8.25 (s, 1H); ESI MS *m/z*: 338 $[M+H]^+$.

*N-(4-((2-(7-Methoxy-2-methylquinolin-4-yl)hydrazono)methyl)-phenyl)methanesulfonamide (**3i**)*

Starting from hydrazine **9e** and aldehyde **10b**, title compound was obtained following the procedure developed for **3a**. Yield: 22%; ^{1}H NMR: (CD_3OD, 300 MHz) δ 2.57 (s, 3H), 3.00 (s, 3H), 3.91 (s, 3H), 7.05 (dd, $J_1=2.4$ Hz, $J_2=9.1$ Hz, 1H), 7.14 (d, $J=2.7$ Hz, 1H), 7.20 (s, 1H), 7.29 (d, $J=8.4$ Hz, 2H), 7.72 (d, $J=8.4$ Hz, 2H), 8.03 (d, $J=9.3$ Hz, 1H), 8.17 (s, 1H). ^{13}C NMR: (CD_3OD, 75 MHz) δ 22.9, 38.3, 54.7, 99.7, 104.7, 110.3, 116.2, 119.8, 122.3, 127.8, 130.9, 140.4, 143.5, 148.6, 149.2, 158.2, 161.4. ESI MS *m/z*: 385 $[M+H]^+$.

*N-(4-((2-(7-Methoxyquinolin-4-yl)hydrazono)methyl)phenyl)-methanesulfonamide (**3j**)*

Starting from hydrazine **9f** and aldehyde **10b**, the title compound was obtained following the procedure developed for **3a** (5 mg, 11% yield); ^{1}H NMR: (DMSO-d_6, 300 MHz) δ 3.00 (s, 3H), 3.84 (s, 3H), 7.03–7.21 (m, 3H), 7.25 (d, $J=8.1$ Hz, 2H), 7.71 (d, $J=7.8$ Hz, 2H), 8.20 (d, $J=9.6$ Hz, 1H), 8.31 (s, 1H), 9.94 (s, 1H), 11.07 (s, 1H); ESI MS *m/z*: 371 $[M+H]^+$.

*N-(4-((2-(Quinolin-4-yl)hydrazono)methyl)phenyl)methanesulfonamide (**3k**)*

Starting from hydrazine **9g** and aldehyde **10b**, the title compound was obtained following the procedure developed for **3a** (13 mg, 32% yield); ^{1}H NMR: (CD_3OD, 300 MHz) δ 3.00 (s, 3H), 7.32 (d, $J=8.4$ Hz, 2H), 7.54 (dd, $J_1=6.1$ Hz, $J_2=16.2$ Hz, 1H), 7.82–7.71 (m, 3H), 7.86 (d, $J=9.1$ Hz, 1H), 8.26 (s, 1H), 8.30 (s, 1H), 8.46 (d, $J=5.7$ Hz, 1H). ESI MS *m/z*: 341 $[M+H]^+$.

*4-(2-(4-(Methylthio)benzylidene)hydrazinyl)quinoline (**3l**)*

Starting from hydrazine **9g** and aldehyde **10c,** title compound was obtained following the procedure developed for **3a** (69 mg, 75% yield); ^{1}H NMR: (DMSO-d_6, 300 MHz) δ 2.52 (s, 3H), 7.35 (d, $J=8.1$ Hz, 2H), 7.63–7.55 (m, 1H), 7.73–7.69 (m, 3H), 7.92–8.08 (m, 2H), 8.64 (s, 1H), 8.84 (s, 2H). ^{13}C NMR: (DMSO-d_6, 300 MHz) δ 14.8, 100.5, 115.8, 120.9, 124.4, 126.3, 127.5, 128.7, 130.5, 134.2, 139.1, 143.1, 143.2, 150.7, 152.9; ESI MS *m/z*: 294 $[M+H]^+$.

Synthesis of compounds 4a–c

*N-(4-((2-(6-Methyl-[1,3]dioxolo[4,5-g]quinolin-8-yl)hydrazinyl)-methyl)phenyl)methanesulfonamide (**4a**)*

To a solution of compound **1** (7 mg, 0.02 mmol) in trifluoroacetic acid (1 mL), triethylsilane (3 μL, 0.04 mmol) was added and the reaction was monitored by TLC until the end of the starting material, then a saturated solution of $NaHCO_3$ was added to the reaction mixture and the organic phase was extracted with EtOAc (3×), dried over Na_2SO_4, filtered and evaporated to dryness. The residue was purified by flash chromatography on silica gel (eluting mixture from 100% $CHCl_3$ to 10% MeOH in $CHCl_3$) to obtain the desired compound **4a** as a yellow oil (6 mg, 75% yield); ^{1}H NMR: (CD_3OD, 300 MHz) δ 2.51 (s, 3H), 2.87 (s, 3H), 4.07 (s, 2H), 6.19 (s, 2H), 7.03 (d, $J=7.5$ Hz, 2H), 7.15 (d, $J=7.8$ Hz, 2H), 7.37 (d, $J=7.8$ Hz, 2H), 7.50 (s, 1H); ESI MS *m/z*: 400 $[M+H]^+$.

*6-Methyl-8-(2-(4-(methylthio)benzyl)hydrazinyl)-[1,3]dioxolo[4,5-g]quinoline (**4b**)*

Compound **4b** was obtained as a brown solid starting from **2a** and following the procedure developed for the preparation of **4a** (17 mg, 72% yield); ^{1}H NMR: ($CDCl_3$, 300 MHz) δ 2.42 (s, 6H), 4.06 (d, $J=5.7$ Hz, 2H), 4.22 (t, $J=5.7$ Hz, 1H), 6.02 (s, 2H), 6.57 (s, 1H), 6.94 (s, 1H), 7.19 (d, $J=8.4$ Hz, 2H), 7.33–7.24 (m, 3H), 7.76 (s, 1H); ESI MS *m/z*: 354 $[M+H]^+$.

*4-((2-(6-Methyl-[1,3]dioxolo[4,5-g]quinolin-8-yl)hydrazinyl)-methyl)benzenesulfonamide (**4c**)*

Compound **4c** was obtained as a brownish solid starting from **3b** and following the procedure developed for the preparation of **4a** (3.6 mg, 90%); ^{1}H NMR: (CD_3OD, 300 MHz) δ 2.52 (s, 3H), 4.19 (s, 2H), 6.19 (s, 2H), 7.04 (d, $J=2.4$ Hz, 2H), 7.49 (s, 1H), 7.59 (d, $J=8.1$ Hz, 2H), 7.81 (d, $J=8.1$ Hz, 2H); ESI MS *m/z*: 387 $[M+H]^+$.

Synthesis of hydrazide 5

*N-(4-(2-(6-Methyl-[1,3]dioxolo[4,5-g]quinolin-8-yl)hydrazine-1-carbonyl)phenyl)methanesulfonamide (**5**)*

To a solution of 4-(methylsulfonamido)benzoic acid **11**[23] (50 mg, 0.23 mmol) in anhydrous DMF (4 mL) at 25 °C, HOBt (31 mg,

Downloaded by [Universita degli Studi di Siena] at 03:47 28 April 2016

0.23 mmol) and DCC (53 mg, 0.25 mmol) were added as solids in small portions. After 30 min the hydrazinoquinoline **9a** (60.8 mg, 0.27 mmol), dissolved in anhydrous DMF (4 mL) was added to the suspension and the reaction mixture was stirred for 12 h at 25 °C. Then, a saturated solution of $NaHCO_3$ was added and the aqueous phase was extracted with EtOAc (3×), dried over Na_2SO_4 and concentrated to dryness. The residue was purified by flash chromatography on silica gel (eluting mixture 5% MeOH in $CHCl_3$) to get title compound as a yellowish oil (6 mg, 6% yield); ^{1}H NMR: (CD_3OD, 300 MHz) δ 2.60 (s, 3H), 2.56 (s, 3H), 6.15 (s, 2H), 7.12 (s, 1H), 7.31 (d, $J = 9.3$ Hz, 2H), 7.58 (s, 1H), 7.76 (d, $J = 8.4$ Hz, 2H), 8.24 (s, 1H); ESI MS *m/z*: 415 $[M + H]^+$.

Synthesis of 4-aminoquinoline derivatives 6–8

*6-Methyl-N-(4-(methylthio)phenethyl)-[1,3]dioxolo[4,5-g]quinolin-8-amine (**6**)*

To a solution of chloride **13** (33 mg, 0.15 mmol) in absolute EtOH at 25 °C, 2-(4-(methylthio)phenyl)ethan-1-amine **12**[24] (25 mg, 0.15 mmol) and Et_3N (62 µL, 0.45 mmol) were added and the reaction was stirred at the same temperature for 76 h. The solvent was evaporated and the residue was purified by flash chromatography on silica gel (eluting mixture 5% MeOH in $CHCl_3$) to obtain the title compound (5 mg, 43% yield); ^{1}H NMR: ($CDCl_3$, 300 MHz) δ 2.47 (s, 3H), 2.57 (s, 3H), 3.03–2.94 (m, 2H), 3.59–3.48 (m, 2H), 6.03 (s, 2H), 6.22 (s, 1H), 6.98 (s, 1H), 7.34–7.10 (m, 6H); ESI MS *m/z*: 353 $[M + H]^+$.

*2-((6-Methyl-[1,3]dioxolo[4,5-g]quinolin-8-yl)amino)ethan-1-ol (**14**)*

A mixture of quinoline **13** (507 mg, 2.29 mmol) in 2-aminoethanol (3 mL) was heated at 150 °C for 15 min and, subsequently, at 190 °C for 30 min. Then the solution was cooled to 25 °C, added of a 10% aqueous solution of $NaHCO_3$ and stirred at 25 °C for 30 min to obtain a precipitate that was filtered and washed with water (4×). The residue was evaporated to dryness to obtain title compound as a brown solid without the necessity of any further purification (296 mg, 52% yield); ^{1}H NMR: (CD_3OD, 300 MHz) δ 2.45 (s, 3H), 3.41 (t, $J = 5.7$ Hz, 2H), 3.81 (t, $J = 5.4$ Hz, 2H), 6.02 (s, 2H), 6.32 (s, 1H), 7.02 (s, 1H), 7.31 (s, 1H); ESI MS *m/z*: 247 $[M + H]^+$.

*6-Methyl-N-(2-(4-(methylsulfonyl)piperazin-1-yl)ethyl)-[1,3]dioxolo[4,5-g]quinolin-8-amine (**7**)*

To a solution of **14** (350 mg, 1.42 mmol) in anhydrous DCM, pyridine (562 mg, 7.1 mmol) was added and the reaction mixture was cooled to 0 °C and added to *p*-toluenesulfonyl chloride (677 mg, 3.55 mmol) in three portions over 5–10 min. The reaction was heated at 50 °C and stirred at that temperature for 4 h, cooled to 25 °C and added to a saturated solution of Na_2CO_3. The aqueous phase was extracted with DCM (3×), dried over Na_2SO_4, filtered and evaporated. The residue was purified by flash chromatography over silica gel (eluting mixture from 100% $CHCl_3$ to 20% MeOH in $CHCl_3$) to obtain 2-((6-methyl-[1,3]dioxolo[4,5-g]quinolin-8-yl)amino)ethyl 4-methylbenzenesulfonate as a yellow-brown oil, that was used immediately in the next step (300 mg, 53% yield); ^{1}H NMR: ($CDCl_3$, 400 MHz) δ 2.29 (s, 3H), 2.50 (s, 3H), 3.68 (br s, 2H), 4.29 (s, 2H), 5.95 (s, 2H), 7.13–7.18 (m, 3H), 7.27 (s, 1H), 7.34 (s, 1H), 7.63 (d, $J = 7.6$ Hz, 2H), 8.57 (s br., 1H); ESI MS *m/z*: 401 $[M + H]^+$. To a solution of the above tosyl compound (156 mg, 0.39 mmol) and **15** (128 mg, 0.78 mmol) in DMSO (1 mL), was added DIPEA (101 µL, 0.58 mmol) and the reaction mixture was heated at 70 °C for 20 h. After cooling to 25 °C, the reaction was added with EtOAc (2 mL) and H_2O (2 mL) and stirred for 15 min. The organic phase was washed with a NaCl saturated solution (5×), dried over Na_2SO_4, filtered and evaporated. The residue was purified by flash chromatography on silica gel (eluting mixture from 100% $CHCl_3$ to 10% MeOH + 1% Et_3N in $CHCl_3$) to obtain the title compound as a white solid (15 mg, 10% yield); ^{1}H NMR: (DMSO-d_6, 400 MHz) δ 2.53–2.57 (m, 7H), 2.66 (t, $J = 8$ Hz, 2H), 2.83 (s, 3H), 3.06 (t, $J = 6$ Hz, 4H), 3.53 (q, $J = 7.2$ Hz, 2H), 6.24 (s, 2H), 6.67 (s, 1H), 7.25 (s, 1H), 7.87 (s, 1H), 8.38 (s br., 1H); ESI MS *m/z*: 393 $[M + H]^+$.

*N-(1-(2-((6-Methyl-[1,3]dioxolo[4,5-g]quinolin-8-yl)amino)ethyl)piperidin-4-yl)methanesulfonamide (**8**)*

To a solution of the tosyl derivative described above (76 mg, 0.19 mmol) in DMSO, the piperidine derivative **16** (70 mg, 0.39 mmol) and DIPEA (48 µL, 0.28 mmol) were added. After 20 h at 70 °C, the reaction mixture was cooled to 25 °C, added with EtOAc (2 mL) and H_2O (2 mL) and stirred for 15 min. The organic phase was washed with a NaCl saturated solution (5×), dried over Na_2SO_4, filtered and evaporated. The residue was purified by flash chromatography on silica gel (eluting mixture from 100% $CHCl_3$ to 10% MeOH + 1% Et_3N in $CHCl_3$) to obtain the title compound as a white solid (20 mg, 26% yield); ^{1}H NMR: (DMSO-d_6, 400 MHz) δ 1.41 (br. s, 2H), 1.76 (br. s, 2H), 2.05 (br. s, 2H), 2.41–2.63 (m, 5H), 2.69–2.88 (m, 5H), 3.08–3.13 (m, 1H), 3.50 (br. s, 2H), 6.23 (s, 2H), 6.64 (s, 1H), 7.00 (br. s, 1H), 7.18 (s, 1H), 7.81 (s, 1H), 8.19 (br s, 1H); ^{13}C NMR: (DMSO-d_6, 75 MHz) δ 20.8, 33.1, 41.7 (2C), 50.4, 52.4, 56.0, 98.7, 98.9, 99.7 (2C), 103.6 (2C), 111.8, 138.0, 147.7, 152.5 (2C), 154.0; ESI MS *m/z*: 407 $[M + H]^+$, 429 $[M + Na]^+$.

Computational details

All calculations performed in this work were carried out on Cooler Master Centurion 5 (Intel Core2 Quad CPU Q6600 @ 2.40 GHz) with Ubuntu 10.04 LTS (long-term support) operating system running Maestro 9.2 (Schrödinger, LLC, New York, NY, 2011) and GOLD 5.2 (Cambridge Crystallographic Data Center, CCDC, UK).

Protein preparation

The three-dimensional structures of MBLs were taken from PDB (2YZ3[25] and 1KO3[26] for VIM-2; 3Q6X[27] for NDM-1; 1DD6[28] for IMP-1). The structures were submitted to protein preparation wizard implemented in Maestro suite 2011 (Protein Preparation Wizard workflow 2011 http://www.schrodinger.com/supportdocs/18/16). This protocol allowed us to obtain a reasonable starting structure of the proteins for molecular docking calculations and/or MD simulation. In particular, we performed three steps to (1) add hydrogens, (2) optimize the orientation of hydroxyl groups, Asn, and Gln, and the protonation state of His, and (3) perform a constrained refinement with the impref utility, setting the max RMSD of 0.30.

3D-chemical databases preparation

Our proprietary database (2300 molecules) was built in Maestro (Maestro, version 9.2 Schrödinger, LLC, New York, NY, 2011). Molecular energy minimizations were performed in MacroModel using the Optimized Potentials for Liquid Simulations-all atom (OPLS-AA) force field 2005[29]. The solvent effects were simulated using the analytical Generalized-Born/Surface-Area (GB/SA) model[30], and no cutoff for nonbonded interactions was selected. Polak-Ribiere conjugate gradient (PRCG) method with 1000 maximum iterations and 0.001 gradient convergence threshold was employed. All derivatives were treated by using LigPrep application (version 2.5, Schrödinger, LLC, New York, NY,

Downloaded by [Universita degli Studi di Siena] at 03:47 28 April 2016

2011), generating the most probable ionization state of any possible enantiomer and tautomer at cellular pH value (7.0 ± 0.5). The resulting output was saved as .sdf file.

HTD protocol

HTD was carried out using GOLD 5.2 (Genetic Optimization for Ligand Docking) software that uses the Genetic algorithm (GA)[31] running under Ubuntu 10.04 LTS OS. This method allows a partial flexibility of protein and full flexibility of ligand. For each of the 30 independent GA runs, a maximum number of 125 000 GA operations were performed. The search efficiency values were set to 100%. The active site radius of 8 Å was chosen by XYZ coordinates from the two metal ions, representing roughly the center of the binding site. Default cutoff values of 2.5 Å (dH-X) for hydrogen bonds and 4.0 Å for van der Waals distances were employed. When the top three solutions attained RMSD values within 1.5 Å, GA docking was terminated. The fitness function ChemScore was employed for ranking the docked compound. In particular the selection of compounds has been performed by applying a ChemScore cutoff value of 40 coupled to visual inspection and clusters analysis (RMSD 0.75 Å as indicated by GOLD software). A cluster was considered relevant for the binding mode of a selected compound if containing at least 25% of docked solutions. For value over 80% of docked solutions found into a single cluster we have reported one representative binding mode. Moreover, all the compounds selected by HTD as potential MBL inhibitors were re-docked during the optimization step by using 100 independent GA run for obtaining more accurate results in order to provide reliable binding modes. The same protocol was also applied to the subsequent compounds obtained during the optimization steps.

Predicted physicochemical properties

QikProp application (QikProp, version 3.4, Schrödinger, LLC, New York, NY, 2011) was used for predicting the physicochemical properties of selected compounds presented in this study.

Prime/MM-GBSA simulation

The Prime/MM-GBSA method implemented in Prime software (Prime, version 3.0, Schrödinger, LLC, New York, NY, 2011) consists in computing the change between the free and the complex state of both the ligand and the protein after energy minimization. The technique was applied using the docking complexes obtained by means of Glide. The software was used to calculate the free-binding energy (ΔG_{bind}) of each ligand, as recently reported by us[32–34].

Enzyme inhibition assays

Purified IMP-1, VIM-2 and NDM-1 MBL enzymes were produced using the *E. coli*-based expression system and purified as previously described[35–37]. Compounds were dissolved in DMSO at the concentration of 100 mM and subsequently diluted in 50 mM HEPES, 50 μM $ZnSO_4$ (pH = 7.5), at a final concentration of 2–5 mM. For poorly soluble compounds, up to 10% DMSO was added to the buffer (the maximum DMSO concentration used in the assay did not affect the enzyme activity). The inhibitory activity of the various compounds on purified MBLs was investigated by measuring the variation of the initial rate of hydrolysis of 90 μM imipenem or 80 μM cefotaxime, used as the reporter substrate, at 30 °C in 50 mM HEPES buffer (pH 7.5) supplemented with 50 μM $ZnSO_4$, in the presence of various inhibitor concentrations. The MBL final concentration in the assays ranged 2.5–40 nM. The K_i value was determined as previously described, using a competitive model of inhibition[38].

In vitro synergistic antibacterial activity

A VIM-2-producing derivative of hyperpermeable *E. coli* AS19 strain (kindly provided by Prof. Nielsen, University of Copenhagen, Denmark and Dr. Good, Royal Veterinary College, London, U.K.) was obtained by electroporation, using the plasmid vector pLBII-VIM-2[39]. The production of the MBL in these strains was verified both by measuring the specific imipenem-hydrolyzing activity of crude extracts, as previously described, and by antimicrobial susceptibility testing (i. e. the determination of β-lactam susceptibility profile of the strains).

The potential synergistic activity of the tested compounds was evaluated by the agar disk diffusion method (in a so-called combo test setup, in which the inhibitor is added to a commercially-available disk already containing the β-lactam antibiotic), and by measuring the diameter of growth inhibition of the β-lactam cefoxitin, in the absence and presence of ≈90 μg of the compounds (added directly to the cefoxitin disk, Oxoid, Milan, Italy). These tests were carried out as recommended by CLSI, using Mueller-Hinton Agar plates[40].

Stability studies

Standard and sample solutions were prepared from a 10 mM DMSO solution of compound **2a**. Three solutions were prepared:

- 250 μM solution in acetonitrile/phosphate buffer 1:1, with a final DMSO content of 2.5% (v/v).
- 250 μM sample solution in acetic acid 50 mM, pH = 3, with a final DMSO content of 2.5% (v/v).
- 250 μM sample solution in distilled water with a final DMSO content of 2.5% (v/v).

Also, the stability of **2a** in acetonitrile solution (1 mg/2 mL) was assessed.

Samples were analyzed (injection volume = 10 μL) at time = 0, 24, 72 h and 5 d using a Shimadzu Prominence apparatus by using a RP-18 Chromolith column (4.6 mm diameter). UV-detection was performed at 254 nm. Elution was performed in a gradient mode (see table below). Retention time = 5.79 min.

Time (min)	CH_3CN (0.1% TFA)	Water (0.1% TFA)	Flow (mL/min)
0	20	80	1.5
10	80	20	1.5

Toxicity studies

Cytotoxicity assays were performed to establish the effect of compound **1** on the mouse fibroblasts NIH3T3 cells. Cell viability was measured by the Neutral Red Uptake (NRU) test and data normalized as % control. For compound **1** TC_{50} NIH3T3 = 25 μM.

Results and discussion

Chemistry

Compounds **2a–e** were prepared as described previously by us[15]. The procedure for the synthesis of novel compounds **3a–l**, **4a–c** and **5** is described in Scheme 1. Final compounds **3a–d**,**f–l** were obtained by reacting hydrazines **9a–g** with equimolar amounts of the suitable carboxaldehydes **10a–c**. The dimethylacetal derivative **3e** was synthesized starting from **2e** by using tetrafluoroboric acid in methanol[41].

The preparation of hydrazine-based compounds **4a–c** envisaged the reduction of the hydrazone double bond, which generally requires a fine-tuning of reducing agent molar ratio

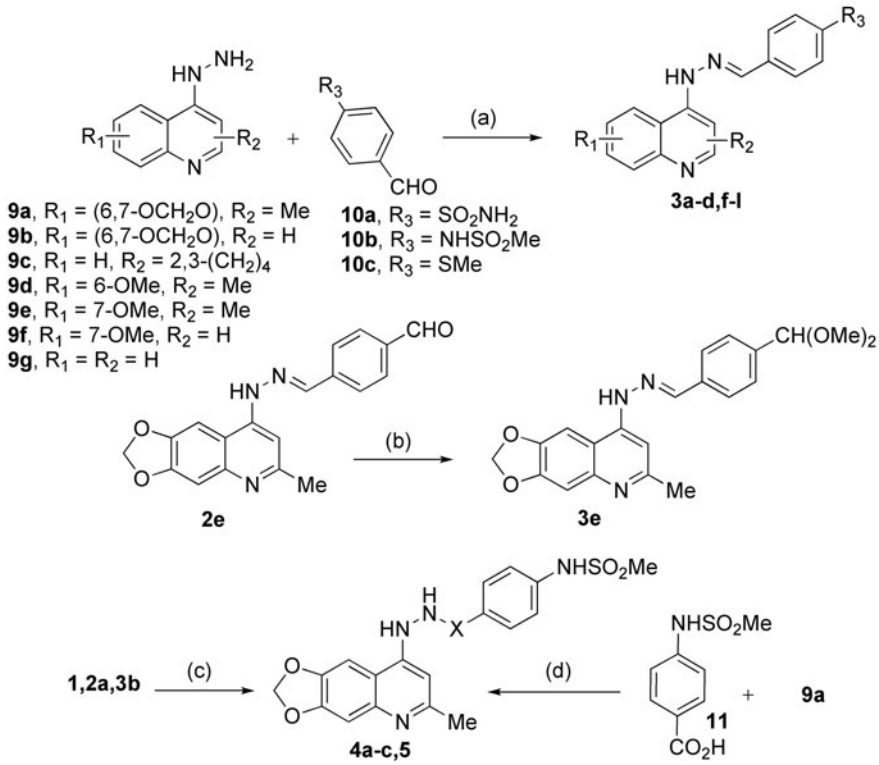

For compounds **3a-l, 4a-c**, and **5**, R_1, R_2 and R_3 and X are defined in Table 2

Scheme 1. Synthetic procedure for the preparation of final compounds **3a–l**, **4a–c**, and **5**. Reagents and conditions: (a) EtOH, reflux, 2–16 h; (b) HBF_4, MeOH, 25 °C, 2 min; (c) Et_3SiH, TFA, 25 °C, 4–6 h; (d) DCC, HOBt, dry DMF, 25 °C, 12 h.

Downloaded by [Universita degli Studi di Siena] at 03:47 28 April 2016

and general reaction parameters (solvent, temperature and time) in order to avoid both too mild and forcing conditions which may be responsible for N–N bond cleavage. In the case of our hydrazine-based compounds, we performed a large series of attempts on compound **2a** in order to find a reliable, repeatable and good-yielding methodology.

Table 1 displays all the major attempts towards this accomplishment and their outputs. As shown, the best reaction conditions identified envisaged the employment of triethylsilane (2 eq) as the reducing agent in the presence of trifluoroacetic acid at 25 °C for 4 h (Table 1, entry 13).

Hydrazide **5** was obtained by coupling carboxylic acid **11**[23] with hydrazine **9a**, in the presence of DCC and HOBt. The synthetic strategy used for the preparation of compounds **6–8** is described in Scheme 2. Chloro-derivative **13** was reacted with alkylamine **12**[24] to furnish derivative **6**. For the synthesis of compounds **7** and **8**, intermediate **13** was reacted with 2-aminoethanol leading to alcohol **14**. This latter was converted into the corresponding tosylate and then reacted with amines **15** and **16** providing final compounds **7** and **8**, respectively. Amines **15** and **16** were prepared through standard functional group interconversion reactions[21,22].

High-throughput docking

The reported X-ray crystal structures of the MBLs IMP-1, VIM-2 and NDM-1 (PDB ID: 1DD6, 3Q6X, and 2YZ3, respectively) were used to implement a HTD campaign[42] performed on a proprietary library of compounds containing around 2300 molecules. The scoring function ChemScore implemented in GOLD software[31,43] was employed during docking protocol in order to rank the best compounds fitting the identified binding site for each enzyme. Compounds showing either a ChemScore >40 for two or three MBLs, or very high ChemScores against one enzyme were taken into consideration. The hits selected based on this protocol were further ranked on the basis of predicted physico-chemical properties and chemical tractability (see Experimental Section for further details). One of the hit compounds (**1**, Figure 1 and Table 2) found by HTD protocol SARs, was chosen for the further studies described here, since it was characterized by (i) good predicted *c*log*P* and *c*log*S* values (2.04 and -4.14, respectively), (ii) molecular weight lower than 400, (iii) low toxicity, (iv) chemical stability (see Experimental Section) and most importantly (v) a low-cost synthetic pathway allowing fast exploration of SARs.

Based on HTD, compound **1** showed interesting binding properties in both VIM-2 (Figure 2A) and NDM-1 (Figure 2B) with a satisfactory ChemScore (41.93 and 40.21, respectively), while a lower ChemScore value was found on IMP-1 (37.42 for the first cluster and 28.71 for the second one; Figure 2C).

The hit compound **1** was tested *in vitro* against all the three MBLs and, coherently with docking studies, was found to be an inhibitor of VIM-2 and NDM-1 in the micromolar range (Table 2) while it did not show appreciable inhibition of IMP-1 at 10 μM (data not shown). Regarding the docking output, **1** presumably interacts with the zinc ions of both VIM-2 and NDM-1 through its methanesulfonamide moiety. In VIM-2 the interaction of the sulfonamide group is further stabilized by a π–π stacking of the aromatic ring with Phe61 (the consensus class B β-lactamase numbering scheme[44] was used throughout). The tricyclic system of **1** forms a potential stacking with Tyr67 side chain in VIM-2 and with Phe70 in NDM-1. Moreover, **1** forms an H-bond with Arg228 of VIM-2 through its hydrazone moiety, and an H-bond with the backbone Lys216 of NDM-1 through the dioxole ring oxygen. This series of contacts, coupled to favourable conformation energies, accounts for the relevant estimated free binding energies of **1** with VIM-2 and NMD-1 ($\Delta G_{bind} = -63.82$ and -59.82 kcal/mol, respectively). On the other hand, as shown in Figure 2 (Panel C), the binding mode of **1** into IMP-1 did not show a docking score comparable to **1** in complex with VIM-2 and NDM-1.

Table 1. Reaction conditions explored for hydrazone bond reduction for conversion of compound **2a** to **4b** (Scheme 1 and Table 2).

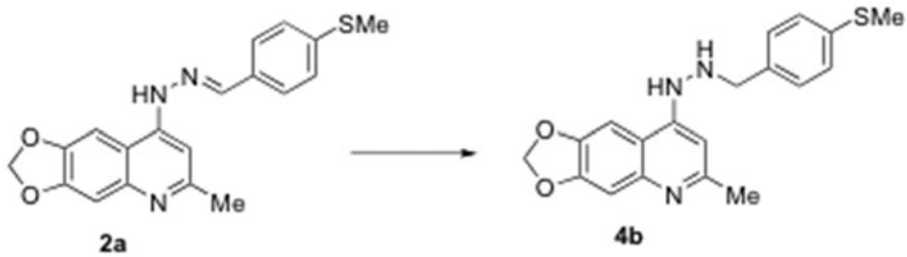

Entry	Reducing agent	Solvent	Temp	Time	Yield
1	$NaBH_4$ (1, 2, 4 or 10 eq)	MeOH	25–70 °C	1–12 h	SM[a]
2	$NaBH_4$ (9 eq)+$TiCl_3$/LiCl/Ni°/$InCl_3$ (3 eq)	MeOH	25 °C	1–18 h	SM
3	$NaBH_4$ (9 eq)+$NiCl_2$ (3 eq)	MeOH/THF 1:1	25 °C	1 h	SM
4	$NaBH_4$ (9 eq)+Ni° (3 eq)	MeOH/4 N NaOH 1:1	60 °C	3–18 h	SM
5	$NaBH_4$ (3 eq)+$TiCl_4$ (1.1 eq)	1,2-dimethoxyethane	25 °C	3 h	Dec.[b]
6	$LiAlH_4$ (3 eq)	THF	0–25 °C	2–18 h	Dec.
7	H_2, Pd/C 10%	MeOH	25 °C	18 h	Dec.
8	Zn (3 eq)	AcOH/H_2O 1:1	60 °C	1–2 h	Dec.
9	$NaBH_4$ (3 eq)	TFA	25 °C	1–18 h	Dec.
10	$NaCNBH_3$ (1 eq)	TFA	25 °C	0.5 h	11%
11	$Na(OAc)_3BH$ (10 eq)	TFA or TFA/DCM 1:5	25 °C	0.5–18 h	4% max
12	Et_3SiH (2 eq)	TFA	25 °C	1 h	SM
13	Et_3SiH (2 eq)	TFA	25 °C	4 h	72%
14	Et_3SiH (2 eq)	TFA	25 °C	18 h	Dec.
15	$(iPr)_3SiH$ (1.1 eq)	TFA	25 °C	4 h	32%
16	$(Cl)_3SiH$ (1.1 eq)	TFA	25 °C	4 h	17%
17	$PhSiH_3$ (1.1 eq)	TFA	25 °C	4 h	24%

[a]SM = only starting material recovered from reaction mixture.
[b]Dec.=decomposition of starting material observed.

Downloaded by [Universita degli Studi di Siena] at 03:47 28 April 2016

Scheme 2. Synthetic procedure for the preparation of final compounds **6–8**. Reagents and conditions: (a) TEA, EtOH, reflux, 76 h; (b) 2-aminoethanol, 150 °C, 15 min then 190 °C, 30 min (c) i. *p*-TsCl, pyridine, dry DCM, 0–25 °C, then 50 °C, 4 h; ii. **15** or **16**, DIPEA, dry DMSO, 70 °C, 20 h.

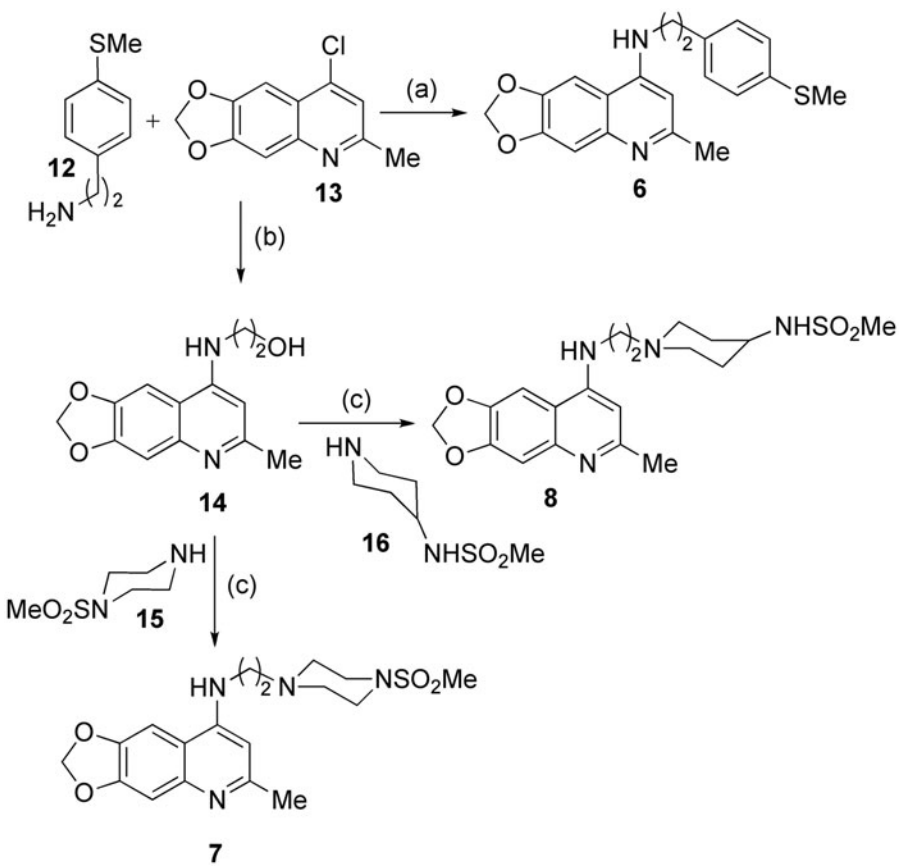

Table 2. K_i values for VIM-2 and NDM-1 for compounds, **1**, **2a–e**, **3a–l**, **4a–c** and **5–8**.

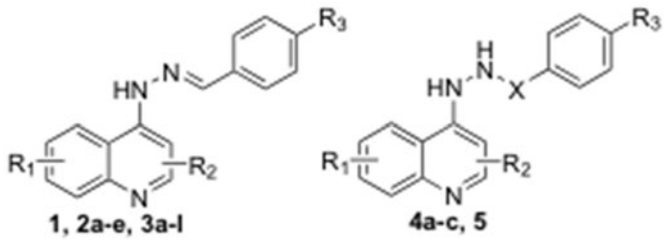

General formula for compounds 6–8 are reported in Scheme 2

Cpd	R_1	R_2	R_3	X	[I]max (μM)	VIM-2 K_i (μM)	NDM-1
1	6,7-OCH_2O-	2-Me	$NHSO_2Me$	–	80–200	10	10
2a	6,7-OCH_2O-	2-Me	SMe	–	50–200	5	N.I.[a]
2b	6,7-OCH_2O-	2-Me	SO_2Me	–	50–200	N.I.	N.I.
2c	6,7-OCH_2O-	2-Me	SOMe	–	80–200	N.I.	N.I.
2d	6,7-OCH_2O-	2-Me	$CH(OEt)_2$	–	80–200	15	–
2e	6,7-OCH_2O-	2-Me	CHO	–	200	10	10
3a	6,7-OCH_2O	2-Me	SO_2NH_2	–	400	17	N.I.
3b	6,7-OCH_2O	H	$NHSO_2Me$	–	100	N.I.	9
3c	6,7-OCH_2O	H	SMe	–	100	10	N.I.
3d	H	2,3-$(CH_2)_4$	$NHSO_2Me$	–	500	24	N.I.
3e	6,7-OCH_2O-	2-Me	$CH(OMe)_2$	–	100	6	N.I.
3f	H	2,3-$(CH_2)_4$	SMe	–	100	2	∼45
3g	6-OMe	Me	$NHSO_2Me$	–	100	5	11
3h	6-OMe	Me	SMe	–	100	9	6
3i	7-OMe	Me	$NHSO_2Me$	–	100	8	9
3j	7-OMe	H	$NHSO_2Me$	–	100	3	N.I.
3k	H	H	$NHSO_2Me$	–	100	N.I.	N.I.
3l	H	H	SMe	–	100	N.I.	N.I.
4a	6,7-OCH_2O	2-Me	$NHSO_2Me$	CH_2	100	N.I.	N.I.
4b	6,7-OCH_2O	2-Me	SMe	CH_2	100	36	13
4c	6,7-OCH_2O	2-Me	SO_2NH_2	CH_2	100	15%	N.I.
5	6,7-OCH_2O	2-Me	$NHSO_2Me$	CO	100-200	N.I.	6
6	–	–	–		100	N.I.	34
7	–	–	–		100	N.I.	N.I.
8	–	–	–		100	N.I.	N.I.

[a]NI, no or poor inhibition. K_i values were not determined for inhibitors showing poor inhibition; in this case, the enzyme inhibition in the presence of the inhibitor at the highest tested concentration (indicated in column 6) was below 20% (residual activity in the presence of inhibitor, ≥80%).

Downloaded by [Universita degli Studi di Siena] at 03:47 28 April 2016

In particular, we have found two main clusters characterized by a strong decrease of computational scores coupled to a weak interaction with the IMP-1 binding site. In fact, despite a similar orientation of **1** into the cleft (first cluster) with the sulfonamide group correctly accommodated close to the two metal ions, only few hydrophobic contacts were established by the tricyclic moiety of **1** with Y181. Moreover, due to this accommodation of the tricyclic ring, the dioxole ring is completely solvent exposed and no other relevant interactions are observed. This binding mode accounts for a docking score of 37.42 and a $\Delta G_{bind} = -38.51$ kcal/mol, indicating a dramatically decreased affinity of **1** for IMP-1, with respect to VIM-2 and NDM-1. The second cluster (Figure 2C) showed a representative binding mode of **1** into IMP-1 with a different orientation in which the molecule appears not to be able to establish any contacts with metals. The only detected polar contact is found between the backbone of S98 and one oxygen from the dioxole ring. Again, this binding mode showed very poor docking score and ΔG_{bind} (28.71 and −32.27 kcal/mol; respectively). The result of the docking studies is in line with the lack of inhibitory activity observed for **1** against IMP-1 (data not shown).

Starting from the hit compound **1**, we embarked in the analysis of the SAR through modification of three structural moieties: (i) the zinc-interacting group, (ii) the dioxoloquinoline ring and (iii) the hydrazone linker (Figure 1) and, due to the lack of activity of **1** against IMP-1, we tested the compounds against VIM-2 and NDM-1 only (results are reported in Table 2).

SAR studies

Zinc-interacting groups

We visually inspected our proprietary library in order to identify analogues of **1** that could share a similar binding mode (**2a–e**)[14] and we synthesized analogues bearing different groups potentially able to interact with the Zn ions (**3a,e**, Table 2). Among these analogues, compound **2a**, bearing a methylthioaryl terminal portion, inhibited VIM-2 with a K_i value of 5 μM while was not active against NDM-1. It is interesting to note that in our calculation, the binding mode of **2a** was similar to **1,** with the methylthio-moiety interacting with the zinc ions (this behaviour is also recapitulated for **3c** and **3f**). In VIM-2 this interaction is further stabilized by a stacking of the aromatic ring with Phe61 while NDM-1 presents an aliphatic residue (Met67) in the corresponding position, and this accounts for lower affinity of **2a**. We also explored the potential of acetal or aldehyde functionalities (**2d,e, 3e**) as terminal zinc binding moieties, potentially able to exploit the Lewis acid properties of the Zn^{2+} ion. The diethylacetale and dimethylacetale containing compounds **2d** and

Downloaded by [Universita degli Studi di Siena] at 03:47 28 April 2016

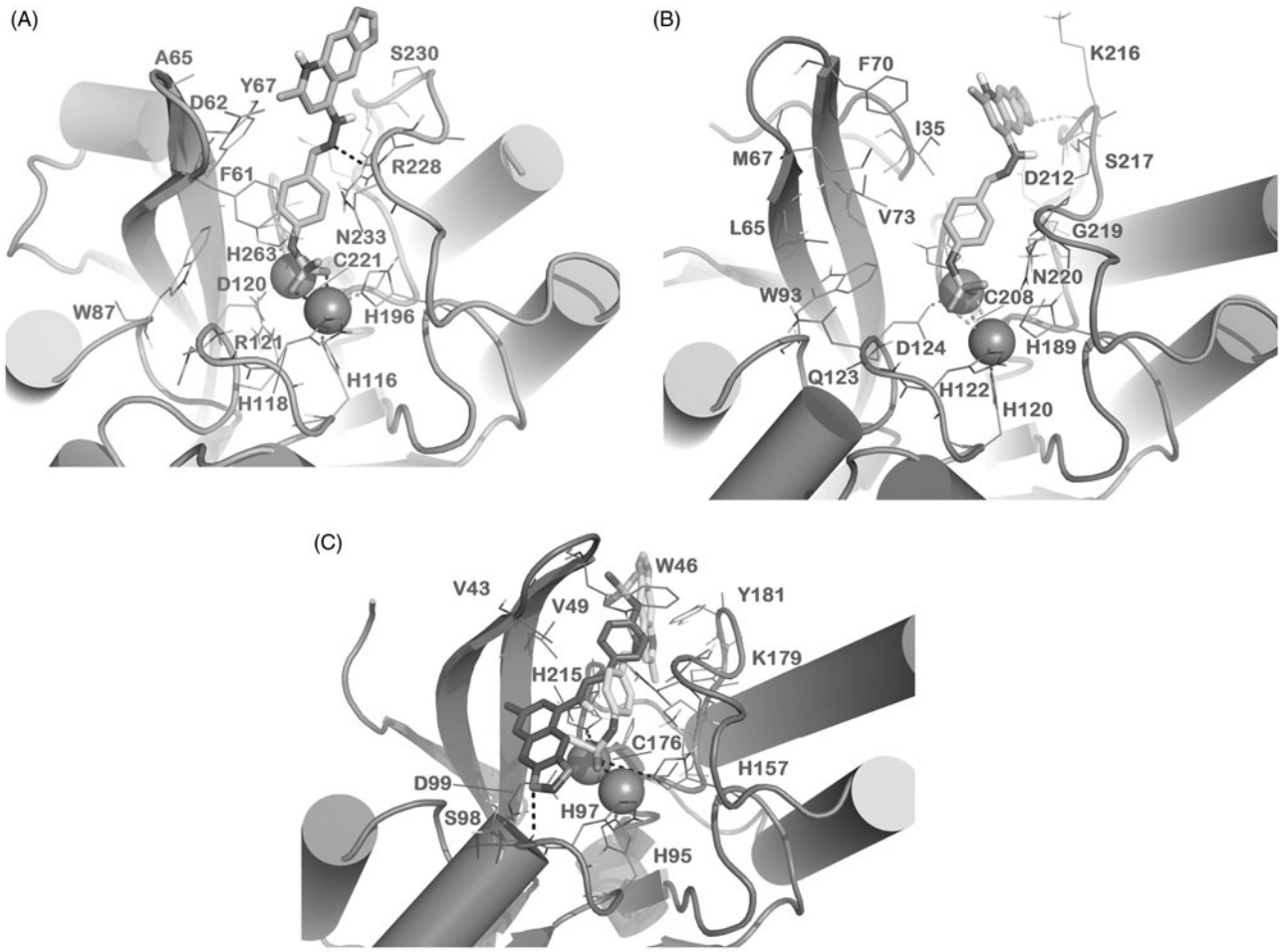

Figure 2. Docked pose of **1** (sticks) into VIM-2 binding site (A), NDM-1 (B) and IMP-1 (C) as found by HTD protocol. Regarding IMP-1, two representative clusters were reported: in light sticks the docked pose of the first cluster, in dark sticks the docked pose of the second cluster. The contacts established by **1** into the active sites of the enzymes are represented by dotted lines. Metal ions were represented by spheres. The numbering of NDM-1 is referred to Uniprot KB protein sequence F6IAY7, while the numbering of IMP-1 is referred to Uniprot KB protein sequence P52699. The contacts established by **1** into the active sites of the enzymes are represented by dotted lines. Metal ions were represented by spheres. The numbering of NDM-1 is referred to deposited Uniprot KB protein sequence F6IAY7. Nonpolar hydrogens were omitted for the sake of clarity. The pictures were generated by PyMOL (The PyMOL Molecular Graphics System, v1.6-alpha; Schrodinger LLC, New York, 2013).

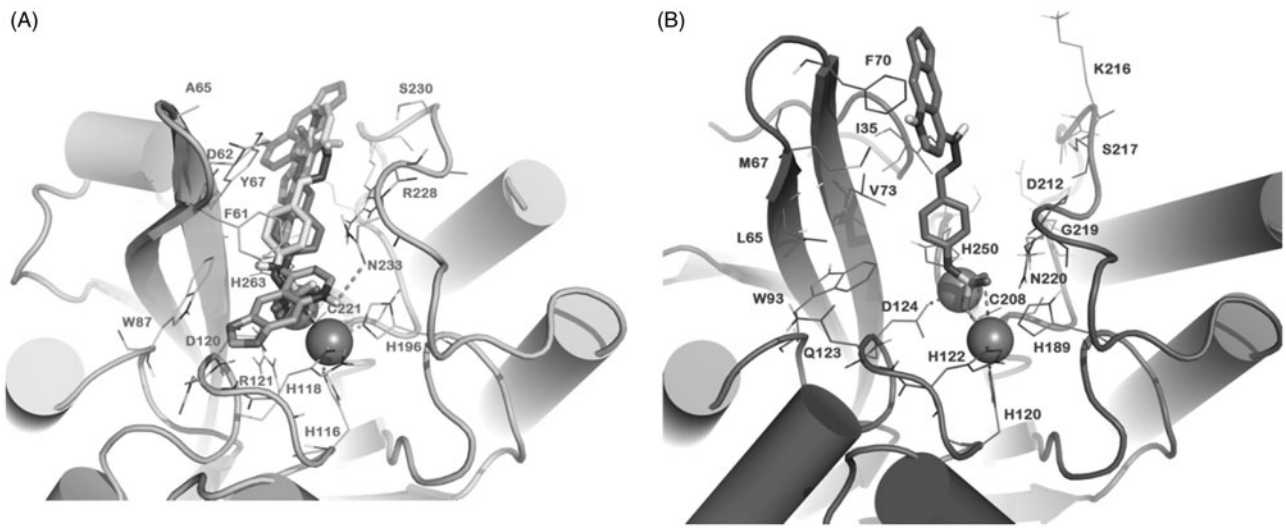

Figure 3. Docked pose of **3b** into VIM-2 binding site (A) and NDM-1 (B) as found by docking protocol. The contacts established by the mentioned compounds into the active sites of the enzymes are represented by dotted lines. Metal ions were represented by spheres. Nonpolar hydrogens were omitted for the sake of clarity. For **3b** in panel A, the clusters are as follows: cluster 1, ChemScore 38.86 and ΔG_{bind} −61.74 kcal/mol; cluster 2, ChemScore 31.79 and ΔG_{bind} −53.29 kcal/mol; cluster 3, ChemScore 27.11 and ΔG_{bind} −40.73 kcal/mol). The pictures were generated using the PyMOL software.

Downloaded by [Universita degli Studi di Siena] at 03:47 28 April 2016

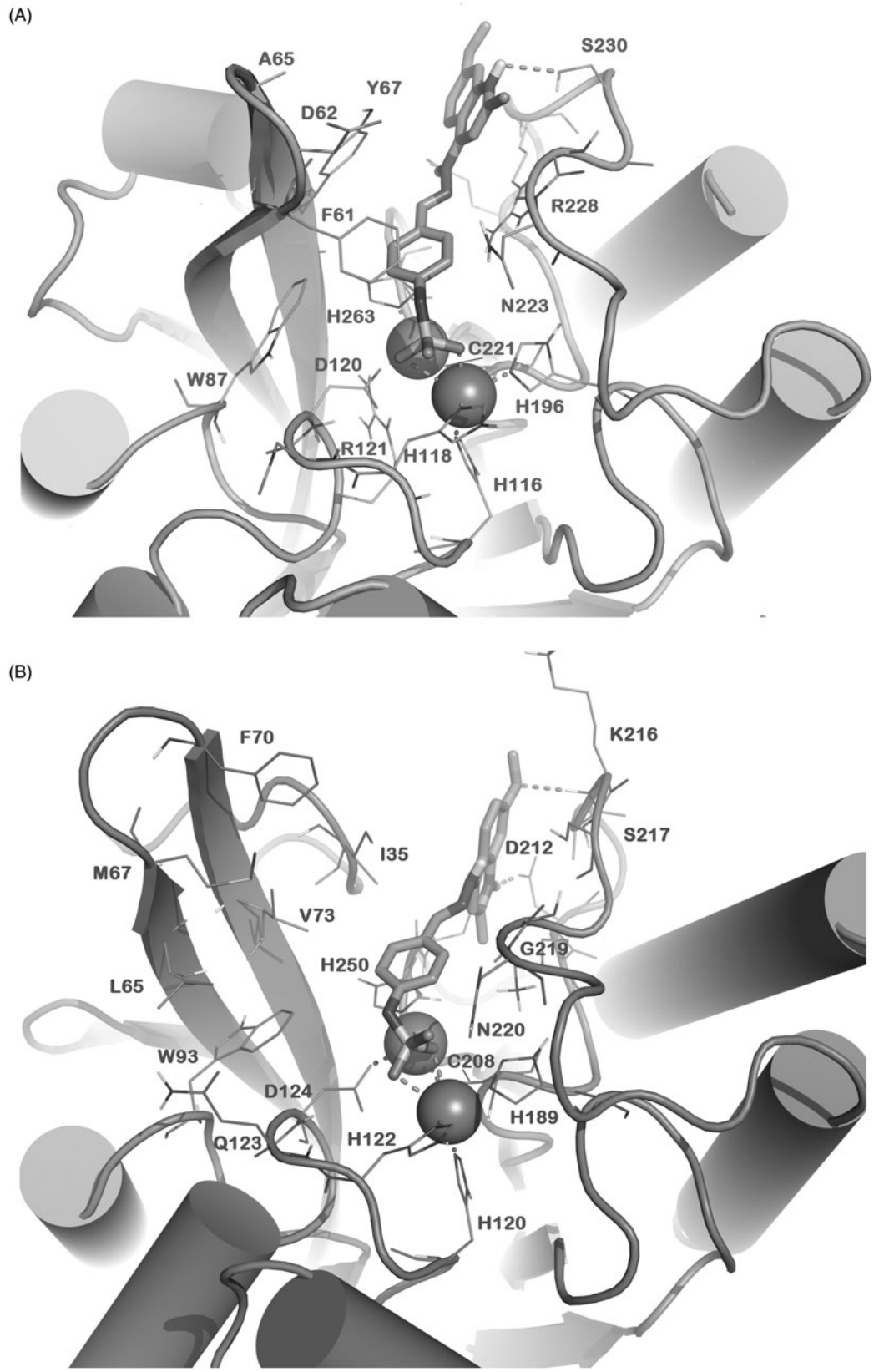

Figure 4. Docked pose of **3i** (sticks) into VIM-2 binding site (A) and NDM-1 (B) as found by HTD protocol. The contacts established by **3i** into the active sites of the enzymes are represented by dotted lines. Metal ions were represented by spheres. The numbering of NDM-1 is referred to deposited protein sequence (Uniprot KB code F6IAY7). Nonpolar hydrogens were omitted for the sake of clarity. The pictures were generated by PyMOL (The PyMOL Molecular Graphics System, v1.6-alpha; Schrodinger LLC, New York, 2013).

3e displayed notable inhibitory activity on VIM-2 isoform (K_i of 15 and 6 μM, respectively). Conversely, aldehyde **2e** was characterized by a comparable inhibitory profile toward both VIM-2 and NDM-1 ($K_i = 10$ μM). The replacement of the *N*-phenylmethanesulfonamide of **1** with a benzenesulfonamide led to compound **3a**, which, although substantially preserving the inhibitory activity towards VIM-2 isoform ($K_i = 17$ μM), completely lost affinity for NDM-1.

Downloaded by [Universita degli Studi di Siena] at 03:47 28 April 2016

Table 3. Synergistic antibacterial activity (combo test agar disk diffusion assay) of selected compounds with cefoxitin on VIM-2-producing *E. coli* AS19 strain.

Compound	Diameter of growth inhibition (mm)
–	19
100% DMSO	19
2a	20
3e	23
3f	19
3g	21
3i	24
3j	23

Quinoline system

Next, we investigated the importance of the methyl substituent at C6 of the dioxoloquinoline system. Compound **3b**, lacking the methyl group at C6 retained affinity for NDM-1 but lost its affinity for VIM-2 (Table 2). Coherently with experimental data, our molecular docking calculation displayed that **3b** is nicely accommodated into the binding site of NDM-1 and the lack of the 6-Me substituent allows the formation of a π–π stacking of the dioxoloquinoline system with Phe70 (Figure 3). In the case of VIM-2, docking of **3b** shows that it can adopt different binding modes in VIM-2, with suboptimal ChemScore and ΔG_{bind} values (Figure 3).

As a further aspect, we considered the output of a different tricyclic moiety in place of the dioxoloquinoline as suggested by docking analysis. In particular, we envisaged the potential of a tetrahydroacridine system[45–48]. However, the tetrahydroacridine-containing compounds **3d,f** maintained the affinity for VIM-2 isoform (K_i = 24 and 2 μM, respectively), while they showed decreased affinity for the NDM-1 MBL.

Taking into account SAR and docking studies, we hypothesized that removal of one oxygen atom from dioxolyl moiety and its replacement with a methoxy group could be well tolerated in both VIM-2 and NDM-1. Consequently, we synthesized a small focused series of analogues (**3g–l**, Table 2) in which differently substituted quinoline systems were coupled to *N*-phenylmethanesulfonamide and phenylthiomethyl moieties, the best performing Zn-interacting groups so far identified. The enzyme inhibitory potencies of the designed compounds are in line with our *in silico* prediction. In particular, as highlighted in Figure 4, compound **3i** was predicted to strongly interact with both MBLs. With respect to VIM-2 isoform (Figure 4A), **3i** showed a binding mode similar to that found for **1** and it also displayed a comparable computational score (ChemScore 39.15, ΔG_{bind} -63.12 kcal/mol). In fact, the metal binding group was correctly positioned by a stacking with Phe61 side chain, and this pose was stabilized by an additional H-bond with Ser230 side-chain. Similarly, **3i** (ChemScore 42.31, ΔG_{bind} −65.16 kcal/mol) docked into NDM-1 was perfectly accommodated for interacting with the metal ion centre and the pose was further stabilized by two H-bonds involving Asp212 and Lys216 (backbone) residues, as shown in Figure 4(B).

Hydrazone linker

The hydrazone bond was then replaced with a hydrazine (**4a–c**), with a hydrazide (**5**), or the entire arylhydrazone system was replaced with alkylamino linker bearing a terminal arylthiomethyl- (**6**), methanesulfonylpiperazin- (**7**) and *N*-(piperidin-4-yl)methanesulfonamide (**8**) moieties. Unfortunately, compounds **4b** and **5** retained activity only against NDM-1, while compounds **4a**,**c** and **6–8** did not show activity against any of the tested MBLs.

Microbiological evaluation

Best performing, compounds **2a** and **3e**,**f**,**g**,**i**,**j** were selected for assessing their ability to potentiate the antibacterial activity of the β-lactam cefoxitin on a VIM-2-producing *E. coli* strain (AS19[pLBII-VIM-2]). As expected, the production of VIM-2 in this *E. coli* laboratory strain confers resistance or decreased susceptibility to most β-lactam antibiotics (data not shown). Interestingly, the antibacterial activity of cefoxitin could be potentiated by the addition of some of the described MBL inhibitors (Table 3). These data highlight that some of the compounds could actually cross the bacterial outer membrane and reach the periplasm to inhibit the MBL, and restore cefoxitin susceptibility of the MBL-producing strain. As getting activity in whole-cell assays might represent a limiting step in compound optimization, our results are encouraging further optimization of these compounds.

Conclusion

In summary, we successfully implemented computational approaches that allowed the identification of compound **1** as a prototypic inhibitor of two MBLs, VIM-2 and NDM-1. SAR studies and rational design led to optimized broad-spectrum MBL inhibitors. Derivatives **3g,i** showed improved activity against the two selected MBLs and **3i** was able to restore β-lactam (cefoxitin) susceptibility in synergistic whole-cell assays, on a VIM-2-producing *E. coli* strain. These *in vitro* data confirm the potential of this class of compounds for the future development of MBL inhibitors.

Acknowledgements

The authors wish to thank Prof. Nielsen (University of Copenhagen, Denmark) and Dr. Good (Royal Veterinary College, London, U.K.) for kindly providing the *E. coli* AS19 strain.

Declaration of interest

Part of this work was supported by the Italian Foundation for Cystic Fibrosis Research with the contribution of Antonio Guadagni&Figli, Delegazione FFC Manciano Grosseto e famiglia Catalano, Hotel Metropole (grants FFC#16/2015 to S.G. and J.-D.D.). The authors report no declarations of interest.

References

1. Gupta V. Metallo beta lactamases in *Pseudomonas aeruginosa* and *Acinetobacter* species. Expert Opin Investig Drugs 2008;17:131–43.
2. King AM, Reid-Yu SA, Wang W, et al. Aspergillomarasmine A overcomes metallo-β-lactamase antibiotic resistance. Nature 2014; 510:503–6.
3. Boucher HW, Talbot GH, Bradley JS, et al. Bad bugs, no drugs: no ESKAPE! An update from the Infectious Diseases Society of America. Clin Infect Dis 2009;48:1–12.
4. Pendleton JN, Gorman SP, Gilmore BF. Clinical relevance of the ESKAPE pathogens. Expert Rev Anti Infect Ther 2013;11:297–308.
5. Wright GD. Molecular mechanisms of antibiotic resistance. Chem Commun (Camb) 2011;47:4055–61.
6. Johnson JW, Gretes M, Goodfellow VJ, et al. Cyclobutanone analogues of beta-lactams revisited: insights into conformational requirements for inhibition of serine- and metallo-beta-lactamases. J Am Chem Soc 2010;132:2558–60.
7. Payne DJ. Microbiology. Desperately seeking new antibiotics. Science 2008;321:1644–5.

Downloaded by [Universita degli Studi di Siena] at 03:47 28 April 2016

8. Bebrone C. Metallo-beta-lactamases (classification, activity, genetic organization, structure, zinc coordination) and their superfamily. Biochem Pharmacol 2007;74:1686–701.
9. Bebrone C, Lassaux P, Vercheval L, et al. Current challenges in antimicrobial chemotherapy: focus on ss-lactamase inhibition. Drugs 2010;70:651–79.
10. von Nussbaum F, Schiffer G. Aspergillomarasmine A, an inhibitor of bacterial metallo-β-lactamases conferring blaNDM and blaVIM resistance. Angew Chem Int Ed Engl 2014;53:11696–8.
11. Crowder MW, Spencer J, Vila AJ. Metallo-beta-lactamases: novel weaponry for antibiotic resistance in bacteria. Acc Chem Res 2006; 39:721–8.
12. Poirel L, Lagrutta E, Taylor P, et al. Emergence of metallo-β-lactamase NDM-1-producing multidrug-resistant *Escherichia coli* in Australia. Antimicrob Agents Chemother 2010;54:4914–16.
13. Li Y, Zhang X, Wang C, et al. Characterization by phenotypic and genotypic methods of metallo-β-lactamase-producing *Pseudomonas aeruginosa* isolated from patients with cystic fibrosis. Mol Med Rep 2015;11:494–8.
14. Zhang YL, Yang KW, Zhou YJ, et al. Diaryl-substituted azolylthioacetamides: inhibitor discovery of New Delhi metallo-beta-lactamase-1 (NDM-1). ChemMedChem 2014;9:2445–8.
15. Gemma S, Giovani S, Brindisi M, et al. Quinolylhydrazones as novel inhibitors of *Plasmodium falciparum* serine protease PfSUB1. Bioorg Med Chem Lett 2012;22:5317–21.
16. Gemma S, Kukreja G, Tripaldi P, et al. Microwave-assisted synthesis of 4-quinolylhydrazines followed by nickel boride reduction: a convenient approach to 4-aminoquinolines and derivatives. Tetrahedron Lett 2008;49:2074–7.
17. Gemma S, Savini L, Altarelli M, et al. Development of antitubercular compounds based on a 4-quinolylhydrazone scaffold. Further structure-activity relationship studies. Bioorg Med Chem 2009;17:6063–72.
18. Fattorusso C, Campiani G, Kukreja G, et al. Design, synthesis, and structure-activity relationship studies of 4-quinolinyl- and 9-acrydinylhydrazones as potent antimalarial agents. J Med Chem 2008;51:1333–43.
19. Cuberes Altisen R, Holenz J, Colombo Piñol M, Port De Pol M. Derivatives of pyrazoline, procedure for obtaining them and use thereof as therapeutic agents. Int. Appl. 2006011005. 02 Feb 2006.
20. Weber V, Rubat C, Duroux E, et al. New 3- and 4-hydroxyfuranones as anti-oxidants and anti-inflammatory agents. Bioorg Med Chem 2005;13:4552–64.
21. Verheijen JC, Yu K, Toral-Barza L, et al. Discovery of 2-arylthieno[3,2-d]pyrimidines containing 8-oxa-3-azabi-cyclo[3.2.1]octane in the 4-position as potent inhibitors of mTOR with selectivity over PI3K. Bioorg Med Chem Lett 2010;20:375–9.
22. Schoenfeld RC, Bourdet DL, Brameld KA, et al. Discovery of a novel series of potent non-nucleoside inhibitors of hepatitis C virus NS5B. J Med Chem 2013;56:8163–82.
23. Greenfield A, Grosanu C. Convenient synthesis of primary sulfonamides. Tetrahedron Lett 2008;49:6300–3.
24. Englert HC, Gerlach U, Goegelein H, et al. Cardioselective K(ATP) channel blockers derived from a new series of m-anisamidoethyl-benzenesulfonylthioureas. J Med Chem 2001;44:1085–98.
25. Yamaguchi Y, Jin W, Matsunaga K, et al. Crystallographic investigation of the inhibition mode of a VIM-2 metallo-beta-lactamase from *Pseudomonas aeruginosa* by a mercaptocarboxylate inhibitor. J Med Chem 2007;50:6647–53.
26. Garcia-Saez I, Docquier JD, Rossolini GM, Dideberg O. The three-dimensional structure of VIM-2, a Zn-beta-lactamase from *Pseudomonas aeruginosa* in its reduced and oxidised form. J Mol Biol 2008;375:604–11.
27. Zhang H, Hao Q. Crystal structure of NDM-1 reveals a common β-lactam hydrolysis mechanism. FASEB J 2011;25:2574–82.
28. Concha NO, Janson CA, Rowling P, et al. Crystal structure of the IMP-1 metallo beta-lactamase from *Pseudomonas aeruginosa* and its complex with a mercaptocarboxylate inhibitor: binding determinants of a potent, broad-spectrum inhibitor. Biochemistry 2000;39:4288–98.
29. Jorgensen WL, Maxwell DS, TiradoRives J. Development and testing of the OPLS all atom force field on conformational energetics and properties of organic liquids. J Am Chem Soc 1996;118:11225–36.
30. Still WC, Tempczyk A, Hawley RC, Hendrickson T. Semianalytical treatment of solvation for molecular mechanics and dynamics. J Am Chem Soc 1990;112:6127–9.
31. Jones G, Willett P, Glen RC, et al. Development and validation of a genetic algorithm for flexible docking. J Mol Biol 1997;267:727–48.
32. Brindisi M, Butini S, Franceschini S, et al. Targeting dopamine D and serotonin 5-HT and 5-HT receptors for developing effective antipsychotics: synthesis, biological characterization, and behavioral studies. J Med Chem 2014;26:9575–97.
33. Brogi S, Butini S, Maramai S, et al. Disease-modifying anti-Alzheimer's drugs: inhibitors of human cholinesterases interfering with β-amyloid aggregation. CNS Neurosci Ther 2014;20:624–32.
34. Giovani S, Penzo M, Brogi S, et al. Rational design of the first difluorostatone-based PfSUB1 inhibitors. Bioorg Med Chem Lett 2014;24:3582–6.
35. Laraki N, Franceschini N, Rossolini GM, et al. Biochemical characterization of the *Pseudomonas aeruginosa* 101/1477 metallo-beta-lactamase IMP-1 produced by *Escherichia coli*. Antimicrob Agents Chemother 1999;43:902–6.
36. Docquier JD, Riccio ML, Mugnaioli C, et al. IMP-12, a new plasmid-encoded metallo-beta-lactamase from a *Pseudomonas putida* clinical isolate. Antimicrob Agents Chemother 2003;47: 1522–8.
37. Borgianni L, Prandi S, Salden L, et al. Genetic context and biochemical characterization of the IMP-18 metallo-beta-lactamase identified in a *Pseudomonas aeruginosa* isolate from the United States. Antimicrob Agents Chemother 2011;55:140–5.
38. Docquier JD, Lamotte-Brasseur J, Galleni M, et al. On functional and structural heterogeneity of VIM-type metallo-beta-lactamases. J Antimicrob Chemother 2003;51:257–66.
39. Borgianni L, Vandenameele J, Matagne A, et al. Mutational analysis of VIM-2 reveals an essential determinant for metallo-beta-lactamase stability and folding. Antimicrob Agents Chemother 2010;54:3197–204.
40. Clinical Laboratory Standard Institute. Performance standards for antimicrobial disk susceptibility tests; approved standard—Twelfth Edition (M02-A12). Wayne, PA, USA; 2015.
41. Kumar D, Kumar R, Chakraborti AK. Tetrafluoroboric acid adsorbed on silica gel as a reusable heterogeneous dual-purpose catalyst for conversion of aldehydes/ketones into acetals/ketals and back again. Synthesis 2008;1249–56.
42. Brindisi M, Brogi S, Relitti N, et al. Structure-based discovery of the first non-covalent inhibitors of Leishmania major tryparedoxin peroxidase by high throughput docking. Scientific Rep 2015;5.
43. Jones G, Willett P, Glen RC. Molecular recognition of receptor sites using a genetic algorithm with a description of desolvation. J Mol Biol 1995;245:43–53.
44. Garau G, Garcia-Saez I, Bebrone C, et al. Update of the standard numbering scheme for class B beta-lactamases. Antimicrob Agents Chemother 2004;48:2347–9.
45. Denny WA. Acridine derivatives as chemotherapeutic agents. Curr Med Chem 2002;9:1655–65.
46. Barros FW, Silva TG, da Rocha Pitta MG, et al. Synthesis and cytotoxic activity of new acridine-thiazolidine derivatives. Bioorg Med Chem 2012;20:3533–9.
47. Butini S, Brindisi M, Brogi S, et al. Multifunctional cholinesterase and amyloid beta fibrillization modulators. Synthesis and biological investigation. ACS Med Chem Lett 2013;4:1178–82.
48. Olszewska P, Mikiciuk-Olasik E, Blaszczak-Swiatkiewicz K, et al. Novel tetrahydroacridine derivatives inhibit human lung adenocarcinoma cell growth by inducing G1 phase cell cycle arrest and apoptosis. Biomed Pharmacother 2014;68:959–67.